

Article

Open Access



Theoretical evidence of self-intercalated 2D materials for battery and electrocatalytic applications

Ke Fan^{1,2}, Yuen Hong Tsang^{1,3,*} , Haitao Huang^{1,2,*}

¹Department of Applied Physics, The Hong Kong Polytechnic University, Hung Hom, Kowloon, Hong Kong 999077, China.

²Research Institute for Smart Energy, The Hong Kong Polytechnic University, Hung Hom, Kowloon, Hong Kong 999077, China.

³Photonic Research Institute, The Hong Kong Polytechnic University, Hung Hom, Kowloon, Hong Kong 999077, China.

***Correspondence to:** Dr. Yuen Hong Tsang, Department of Applied Physics, The Hong Kong Polytechnic University, 11 Yuk Choi Rd, Hung Hom, Kowloon, Hong Kong 999077, China. E-mail: yuen.tsang@polyu.edu.hk. Prof. Haitao Huang, Department of Applied Physics, The Hong Kong Polytechnic University, 11 Yuk Choi Rd, Hung Hom, Kowloon, Hong Kong 999077, China. E-mail: aphhuang@polyu.edu.hk

How to cite this article: Fan K, Tsang YH, Huang H. Theoretical evidence of self-intercalated 2D materials for battery and electrocatalytic applications. *Energy Mater* 2023;3:300047. <https://dx.doi.org/10.20517/energymater.2023.43>

Received: 2 Jun 2023 **First Decision:** 13 Jul 2023 **Revised:** 29 Jul 2023 **Accepted:** 7 Aug 2023 **Published:** 2 Nov 2023

Academic Editor: Hao Liu **Copy Editor:** Fangling Lan **Production Editor:** Fangling Lan

Abstract

Covalently bonded two-dimensional (2D) self-intercalated transition metal chalcogenides (i.e., ic-2Ds) have been recently fabricated experimentally, and their properties are highly tunable by stoichiometry and composition. Inspired by this progress, we focus on the applications of ic-2Ds in the field of electrochemistry and systematically investigate their performance in lithium-ion batteries (LIBs) and electrocatalytic hydrogen evolution reactions (HER). By means of density functional theory calculations, seven 3d-metal ic-2Ds are confirmed to be thermodynamically, mechanically, and thermally stable. The metallicity and abundant active sites endow these ic-2Ds with the potential as excellent electrode materials and HER catalysts. Among them, Ti_7S_{12} and V_7S_{12} exhibit the potential as anode materials for LIBs, showing low Li diffusion energy barriers, suitable open-circuit voltages, and ultrahigh capacity of 745.6 and 723.9 mA hg⁻¹, respectively; Cr_7S_{12} and Co_7S_{12} show promises for HER with moderate hydrogen adsorption strengths. This theoretical study provides a new avenue for the application of newly reported ic-2Ds in various electrochemical energy conversion and storage applications.

Keywords: Self-intercalated 2D materials, transition metal chalcogenides, lithium-ion batteries, hydrogen evolution reaction



© The Author(s) 2023. **Open Access** This article is licensed under a Creative Commons Attribution 4.0 International License (<https://creativecommons.org/licenses/by/4.0/>), which permits unrestricted use, sharing, adaptation, distribution and reproduction in any medium or format, for any purpose, even commercially, as long as you give appropriate credit to the original author(s) and the source, provide a link to the Creative Commons license, and indicate if changes were made.



INTRODUCTION

Due to the limited resources of fossil fuels and the increasing demand for energy, the development of potential energy alternatives to conventional fuels and the corresponding energy storage technologies has become a major global concern^[1-4]. Among them, lithium-ion batteries (LIBs) have attracted widespread attention as one of the most successful clean energy storage technologies^[5-8]. However, their activity is currently hampered by relatively poor rate capability and low capacity. Extensive research work has demonstrated that the rational design of electrode materials may be a compelling way to improve battery performance. In addition, hydrogen is equally worthy of extensive research as a potential energy resource for substituting conventional fossil fuels^[9-14]. Water electrolysis offers an environmentally friendly and sustainable way to generate hydrogen via hydrogen evolution reactions (HER). It is worth noting that HER usually exhibits a high overpotential, which significantly hinders the efficiency of water splitting. Therefore, the rational design of highly efficient electrocatalysts to facilitate the HER process is an urgent issue.

Two-dimensional (2D) transition metal dichalcogenides (TMDs) are one of the most important classes of 2D materials. They exhibit the general formula of MX_2 , where M represents a transition metal, and X denotes a chalcogen (S, Se, Te) atom^[15-17]. The layered structure of TMDs endows strong covalent bonding (in-plane) and weak van der Waals (vdW) interaction (interlayer) characteristics, giving TMDs sufficient interlayer spaces for intercalating guest ions or molecules, which is beneficial for fast ion diffusion and charge transport along the channels, making TMDs highly advantageous for battery application. Besides, the wide exposure of active sites on the surface of 2D TMDs is also beneficial for electrocatalytic applications. Recently, researchers have found that filling the vdW gap of TMDs with intercalants can be a good way to tune their electrochemical performance. To date, most works focus on the intercalation of foreign atoms into the vdW gap^[18-20]. For instance, Attanayake *et al.* systematically investigated the effect of cation (Na^+ , Ca^{2+} , Ni^{2+} , and Co^{2+}) intercalation into the MoS_2 interlayer both experimentally and computationally^[18]. Compared to pure MoS_2 , the intercalated 1T- MoS_2 showed an increase in current density and a decrease in HER overpotential. Wu *et al.* found that the intercalation of lithium (Li) atoms into the 2H- MoS_2 interlayer would induce a phase transition from 2H- to 1T- MoS_2 , which greatly affects the electronic properties of the system^[21]. Therefore, the adsorption of an appropriate quantity of foreign metal atoms on TMDs can modulate the electron density, resulting in a beneficial tuning of the activity in electrocatalytic reactions. However, the number of intercalants is limited by the size of the guest species, and the intercalation of foreign atoms may bring extra crystalline imperfections. Recently, Zhao *et al.* realized the self-intercalation of TMDs, with native metal atoms introduced into the bilayer TMDs with the intercalated extent σ between 25% and 100% (25%, 33.3%, 50%, 66.7%, and 100%) for the first time, and they named these self-intercalated 2D materials as ic-2Ds^[22]. Studies have shown that self-intercalation can adjust many physical and chemical properties and bring in new phenomena to TMDs, such as ferromagnetism^[22]. Nevertheless, a systematic investigation of the electrochemical applications of these ic-2Ds in batteries and electrocatalysts has not yet been reported, which is definitely interesting, considering the tunable properties through the manipulation of ic-2D compositions.

In this work, we use first-principles calculations to study the properties of seven 3d-metal ic-2D materials with the content of $\sigma = 33\%$ (i.e., M_7S_{12} , $M = Ti, V, Cr, Mn, Fe, Co,$ and Ni) and evaluate their application as anode materials in LIBs and HER process. We find that atomic intercalation can give rise to ferromagnetism, such as in the case of Co_7S_{12} . Among them, Ti_7S_{12} and V_7S_{12} are highly promising as anode materials of LIBs, which exhibit small Li diffusion barriers and high capacities. With regard to the HER catalytic activity, Cr_7S_{12} and Co_7S_{12} show high performance at a low hydrogen coverage (θ). This work exemplifies the 3d ic-2Ds as highly potential energy conversion and storage materials and calls for more research efforts on exploring ic-2Ds in other related fields^[23].

COMPUTATIONAL METHODS

Our density functional theory (DFT) calculations were performed by the Vienna *ab initio* simulation package (VASP)^[24]. The exchange-correlation function was described by the generalized gradient approximation with the Perdew-Burke-Ernzerhof flavor^[25]. Spin-polarization was considered for the systems with non-zero magnetic moments. For the geometry relaxation, the kinetic energy cutoff was set as 600 eV, and the energy/force convergence criteria were 10^{-6} eV and 0.01 eV \AA^{-1} , respectively. The Monkhorst-Pack k -point grids of $9 \times 9 \times 1$ were used for the unit cell, while $3 \times 3 \times 1$ grids were used for the $2 \times 2 \times 1$ supercell. A 20 \AA vacuum layer was introduced in order to avoid the spurious interaction between adjacent layers. The vdW interaction was taken into account by using Grimme's DFT-D2^[26] approach. The Bader charge analysis^[27] was used to estimate the amount of charge transfer quantitatively. Furthermore, the climbing image nudged elastic band (CI-NEB) method^[28] was used to calculate the minimum diffusion energy barrier. To investigate the thermal stability, *ab initio* molecular dynamics (AIMD) simulations^[29] were performed with the time step of 2 fs at 300 K.

As an anode of LIBs, ic-2Ds can store Li atoms via the following chemical reaction,



Then, the lithium adsorption energy E_{ad} on the ic-2D surface can be defined as:

$$E_{ad} = E_{M_7S_{12}Li_n} - E_{M_7S_{12}} - nE_{Li} \quad (2)$$

where $E_{M_7S_{12}Li_n}$ is the total energy of ic-2D with n Li atoms adsorbed, $E_{M_7S_{12}}$ denotes the DFT-calculated total energy of the pristine ic-2D crystals, and E_{Li} is the DFT-calculated total energy of one Li atom in the lithium *bcc* bulk. An open-circuit voltage (OCV) is a crucial indicator to determine the capacity of battery materials; average OCV within the adatoms coverage range of $n_1 \leq n \leq n_2$ can be estimated by

$$OCV \approx \frac{E_{M_7S_{12}Li_{n_1}}(n_1) - E_{M_7S_{12}Li_{n_2}}(n_2) + (n_2 - n_1)E_{M_7S_{12}}}{(n_2 - n_1)} \quad (3)$$

where $E_{M_7S_{12}Li_{n_1}}$ and $E_{M_7S_{12}Li_{n_2}}$ are the total energies of the substrate with adatom (n_1 and n_2 adsorbed contents, respectively). The theoretical capacity (C) is defined as:^[30,31]

$$C = znF/M_{M_7S_{12}} \quad (4)$$

where z is the valence number, n represents the maximum adatom content, F is the Faraday constant (26.8 A h mol^{-1}), and $M_{M_7S_{12}}$ is the relative molecular mass of M_7S_{12} .

The Gibbs free energy changes (ΔG) for hydrogen adsorption were calculated by the following formula^[32,33]

$$\Delta G = \Delta E + \Delta ZPE - T\Delta S + \Delta G_{pH} \quad (5)$$

where ΔE , ΔZPE , $T\Delta S$, and ΔG_{pH} denote the changes of total energy calculated by DFT, zero-point energy, entropic contribution, and pH contributions, correspondingly. The zero-point energy and entropic contribution are calculated from the DFT-calculated vibrational frequencies, and the temperature is set as 298 K. ΔG_{pH} was calculated as 0.059 pH, and pH = 0 was used in the calculations.

RESULTS AND DISCUSSION

Geometric structures and stabilities of the ic-2D materials

The ic-2D crystals consist of two layers of TMDs and one layer of transition metal intercalants, which are native. The MX_2 monolayer has a sandwiched structure, and the M layer is sandwiched between the two X layers, as shown in [Figure 1A](#). The weak vdW bonding between the two TMD layers allows M atoms to insert and occupy the gap and locate at the octahedral vacant sites. Distinct stoichiometric phases are, therefore, produced depending on the different levels of intercalation. In this way, the chemical formula can be generally expressed as $\text{M}_\sigma\text{M}_2\text{X}_4$ for ic-2D crystals, where σ represents the concentration of intercalated ions. In this work, we focus on seven different 1T phase $3d$ transition metal sulfides with $\sigma = 33\%$ in ic-2Ds: M_7S_{12} ($\text{M} = \text{Ti}, \text{V}, \text{Cr}, \text{Mn}, \text{Fe}, \text{Co}, \text{and Ni}$). For M_7S_{12} , the vertical distance between the top and bottom sulfur layers is denoted as height h , while the bond lengths of M-S bonds are denoted as d_1 - d_3 , [[Figure 1A](#)], and the results for all the ic-2Ds are summarized in [Supplementary Table 1](#). To screen out ic-2Ds with high stability for potential applications as Li-ion anodes and HER electrocatalysts, we utilize the screening procedure described in [Figure 1B](#): first, thermodynamic, mechanical, and thermal stabilities of ic-2Ds are checked, followed by investigating their electrode and electrocatalytic performance.

Before studying the specific properties of a certain 2D material, stability is always the first thing we should consider. Herein, the thermodynamic, mechanical, and thermal stabilities of ic-2Ds are evaluated. First, negative cohesive energy (E_{coh}) is used as the condition to judge whether 2D materials are thermodynamically stable. From our results, all seven ic-2D systems can satisfy the thermodynamic criteria for stability, lying in the range between -4.08 and -6.45 eV/atom [[Supplementary Table 2](#)], indicating that they are feasible in experiments. Second, the mechanical stability is examined by calculating their 2D elastic constants by DFT. Using the Born-Huang criteria: $C_{11}C_{22} - C_{12}^2 > 0$ and $C_{66} > 0$ [[Supplementary Table 3](#)]^[34], we find that all the systems can satisfy the criteria and thus are mechanically stable. Finally, the thermal stability of the material is proved by performing a series of AIMD simulations at 300 K with a time step of 2 fs. After performing AIMD simulations for 10 ps, no significant structural collapse or deformation can be found, and the total energy and temperature of the system tend to oscillate around the equilibrium values, indicating thermal stability [[Supplementary Figure 1](#)]^[35-37].

The comprehensive assessment of stability discussed above demonstrates that all the seven systems are feasible for experimental synthesis (in fact, three of them have already been fabricated, which are V_7S_{12} , Cr_7S_{12} , and Fe_7S_{12})^[22], and the optimized structures of these ic-2D systems are shown in [Supplementary Figure 2](#). Due to the insertion of native transition metal atoms, ic-2Ds exhibit pseudo-2D structures, and some of them also exhibit anisotropic characters, such as V_7S_{12} , Cr_7S_{12} , and Mn_7S_{12} [[Supplementary Table 1](#)], which may originate from the lowering of symmetry due to their self-intercalation nature. Typically, the seven ic-2Ds have lattice constants (a , b), ranging from 5.5 to 6.0 Å, heights (h) between 7.2 and 8.7 Å, and metal-sulfur bond lengths (d) between 2.2 and 2.5 Å.

To further understand the origin of the high stability of ic-2Ds, differential charge density (DCD) and electron localization functions (ELF) are performed to investigate the bonding properties of ic-2Ds. DCD ($\Delta\rho$) is defined as $\Delta\rho = \rho_{\text{M}_7\text{S}_{12}} - \rho_{\text{M}_6\text{S}_{12}} - \rho_{\text{M}}$, and the DCD plots in [Figure 2A](#) and [Supplementary Figure 3](#) indicate significant charge transfer between the M and the surrounding S atoms. Taking Co_7S_{12} as an

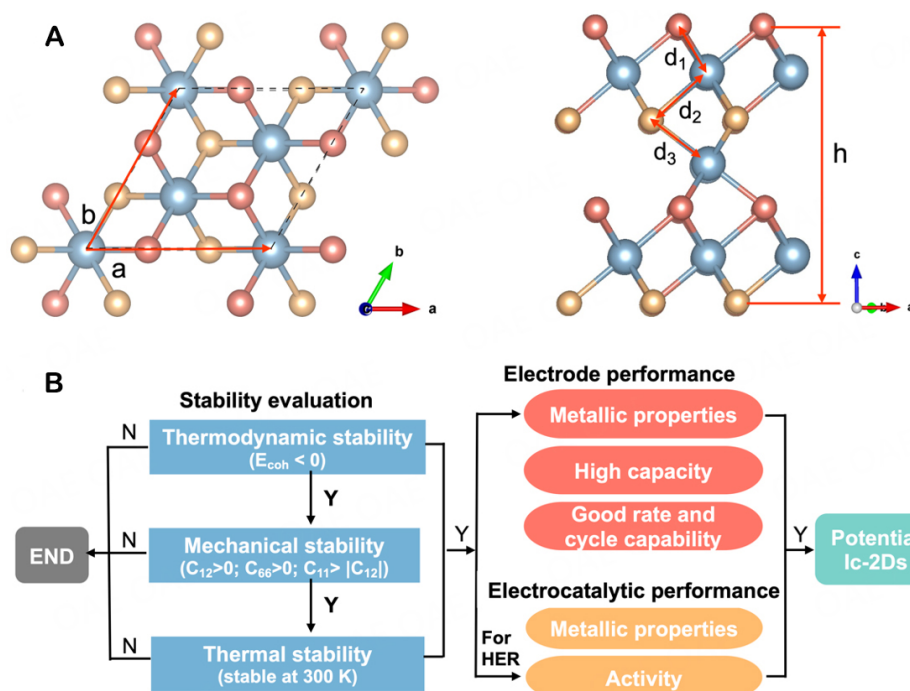


Figure 1. (A) Representative geometric structure of the M_7S_{12} ic-2Ds ($\sigma = 33\%$) from the top and the side views. M atoms are denoted in blue, and S atoms are denoted in orange for the first layer and yellow for the second layer in each MS_2 layer for better visual distinction, respectively. (B) Procedure to screen potential ic-2D electrode materials and HER electrocatalysts.

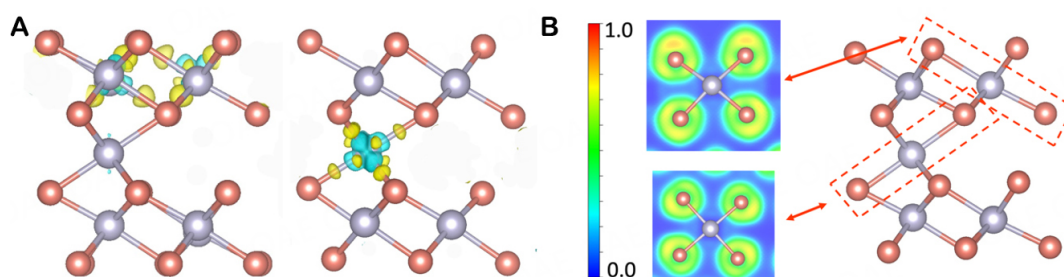


Figure 2. Bonding properties of Co_7S_{12} . (A) Differential charge density distributions of Co_7S_{12} , where the isosurface value is set as $0.012 e/Bohr^3$. Yellow and green colors represent charge accumulation and depletion, respectively. (B) ELF maps of Co_7S_{12} . The values of ELF > 0.5 , ELF = 0.5, and ELF < 0.5 represent the covalent bond, metallic bond, and ionic bond, respectively. Co atoms and S atoms are denoted in purple and orange, respectively.

example [Figure 2A], the difference in local bonding arrangement can induce strong charge transfer from the cobalt atom to the nearby sulfur atom (for Co atoms in both the pristine CoS_2 layer and the intercalated layer). The ELF plots in Figure 2B further demonstrate that most electrons are located around the sulfur atoms, which reveals the ionic character of cobalt-sulfur bonds in Co_7S_{12} . The significant ionic bond contributes to its robust structural stability, and these phenomena can also be observed in other ic-2D systems [Supplementary Figures 3 and 4].

Electronic and magnetic properties of ic-2Ds

For the TMD materials, the electronic structure has been proven to be strongly dependent on the number of d-electrons and the coordination environment of the transition metal atoms^[38-40]. For example, 2H-MoS₂ exhibits semiconducting nature with a band gap of about 1.3 eV, and this can be attributed to the

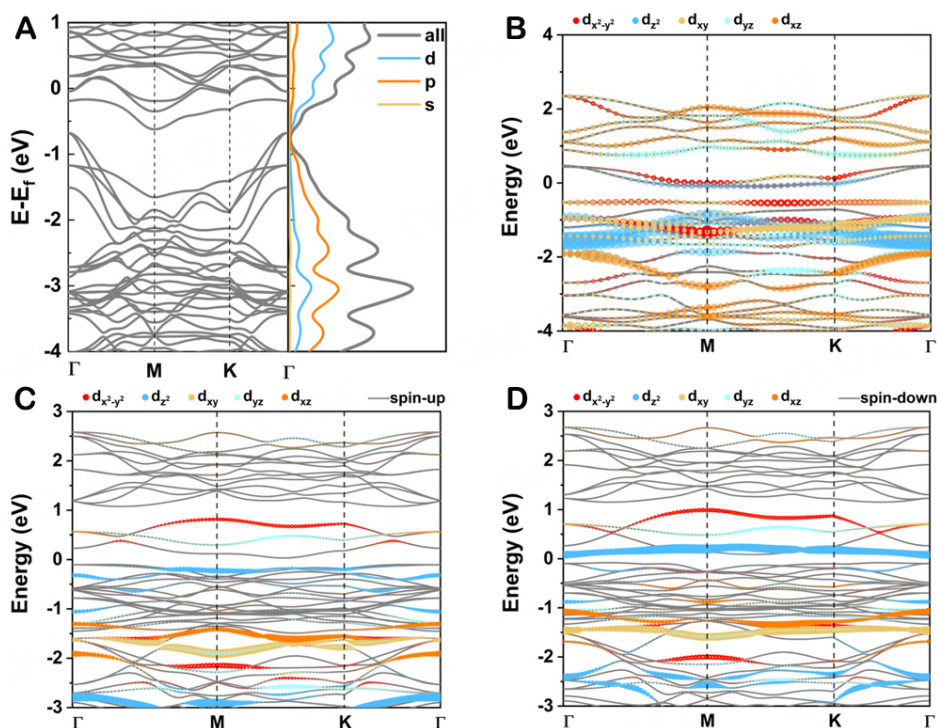


Figure 3. (A) Electronic band structures and DOS plots of Ti_7S_{12} . (B) The orbital-resolved band structure of pristine 1T- CoS_2 . (C and D) The orbital-resolved and spin-resolved band structures of Co_7S_{12} (left: spin-up; right: spin-down).

symmetry-induced splitting of the Mo $4d$ orbitals with the fully occupied Mo $4d_{z^2}$ orbitals and unoccupied Mo $4d_{xy}/d_{x^2-y^2}$ ^[41,42]. However, for the metallic feature 1T- MoS_2 monolayer, the Mo $4d$ orbitals split into the partially filled $4d_{xy}/d_{yz}/d_{xz}$ orbitals and non-occupied Mo $4d_{z^2}$ and Mo $4d_{x^2-y^2}$ levels. Thus, altering the coordination environment of the transition metal atoms may lead to the rearrangement of d electrons, giving rise to distinct electronic or magnetic properties.

Here, for the ic-2D systems, as revealed by the electronic density of states (DOS) and band structure calculations, all the ic-2D systems exhibit metallicity. Taking the case of Ti_7S_{12} as an example, the metallic behavior is revealed by the Fermi level (E_F) crossing through the electronic bands, and this is mainly contributed by the Ti d orbitals [Figure 3A]. A similar phenomenon is found in the other six ic-2D systems [Supplementary Figure 5]. We also inspect the magnetic properties of ic-2Ds. Among the seven systems, non-zero magnetic moments can be found in five of them, i.e., V_7S_{12} , Cr_7S_{12} , Mn_7S_{12} , Fe_7S_{12} , and Co_7S_{12} , and they exhibit a ferromagnetic ground state (GS). Interestingly, the ferromagnetic property of Co_7S_{12} is solely induced by the intercalated Co atom since the perfect monolayer 1T CoS_2 possesses a non-magnetic GS. In the pristine 1T CoS_2 system, the electronic states at E_F mainly consist of cobalt- d_z^2 , cobalt- $d_{x^2-y^2}$, and cobalt- d_{xy} orbitals [Figure 3B]. For Co_7S_{12} , on the other hand, the intercalated cobalt atoms introduce additional bands (spin-split bands) across the E_F , and a magnetic GS, therefore, develops [Figure 3C and D]. Moreover, the introduced magnetic moments are mainly localized on the d orbitals of the intercalated cobalt atom, and the net magnetic moment is calculated as $1.17 \mu\text{B}/\text{unit cell}$, which correlates with a large degree of charge transfer, nearly $0.6 |e|$ between the inserted Co and the surrounding S atoms as calculated by Bader charge analysis [Supplementary Figure 6]. On the other hand, V_7S_{12} , Cr_7S_{12} , Mn_7S_{12} , and Fe_7S_{12} have ferromagnetic 1T-phase MS_2 , and their ferromagnetism is contributed by both the intercalated ions and the pristine layers.

Performance as anode materials for LIBs

The predicted ic-2D crystals exhibit a morphology rather similar to TMDs, which endows them with similar characteristics such as high specific surface area and metallic features, encouraging us to investigate their capability as anodes for LIBs.

In order to study the properties of lithium adsorption on ic-2Ds, a $2 \times 2 \times 1$ supercell is applied to investigate the possible lithium adsorption sites. Six high-symmetry adsorption sites on the surface, as well as the intercalated layer of ic-2D crystals, are considered [Supplementary Figure 7], and the adsorption property and favorable adsorption sites are investigated by comparing their adsorption energies E_{ad} quantitatively. The results show that a single Li atom prefers to be adsorbed on the S5 site for Ti_7S_{12} , V_7S_{12} , Mn_7S_{12} , and Ni_7S_{12} and on the S1 site for Cr_7S_{12} , Fe_7S_{12} , and Co_7S_{12} [Supplementary Table 4].

To explore the maximum theoretical capacity of ic-2D, layers of Li atoms are gradually added to the system. If we take Ti_7S_{12} as an example, the first lithium layer prefers to be intercalated on the energetically most favorable S5 sites, followed by the redetermined S1 sites, and the third and fourth lithium layers are on the S6 and S4 sites, respectively [Figure 4A]. After layers of Li atoms are adsorbed on both sides of Ti_7S_{12} crystals, the OCVs calculated with the number of Li layers ranging from one to seven are 3.8, 2.1, 1.7, 1.1, 0.9, 0.8, and 0.7 V, correspondingly [Supplementary Figure 8]. These positive OCV values suggest that seven lithium layers can be adsorbed on Ti_7S_{12} ic-2D with high stability, and this corresponds to a high theoretical capacity value of 745.6 mA hg^{-1} [Figure 4B]. As a comparison, the value for the commercialized graphite anode is only 372 mA hg^{-1} . In addition, due to the long distance between the third lithium layer and the ic-2D substrate, the chemical interactions between them are very weak, so the outer lithium layer is not further considered. A similar feature is observed in V_7S_{12} [Supplementary Figure 9]. It should be noted that other systems cannot host up to seven layers of Li atoms owing to the collapse of the crystal structures. For instance, Co_7S_{12} and Ni_7S_{12} can only hold three and four layers, respectively.

The metal ion diffusion is directly related to the cycle and rate capability of batteries. Herein, the climbing-image nudged elastic band method is used to study the Li diffusion process from one lithium adsorption site in the most energetically favorable configuration to the most neighboring stable site on both the surface and the intercalated layer [Figure 5]. For the surface diffusion process, we consider three different diffusion paths, which are denoted as path one, path two, and path three by red, black, and blue arrows, respectively [Figure 5A], which connect the two neighboring most preferred adsorption sites. For all the seven systems, the lowest diffusion barriers are calculated to be along path 1, and the values range from 0.17 to 0.69 eV; on the other hand, for the interlayer diffusion pattern, the calculated energy barriers are much higher, ranging from 0.58 to 1.58 eV, where Li diffusion on V_7S_{12} , Cr_7S_{12} , Mn_7S_{12} , Fe_7S_{12} , and Co_7S_{12} is along path 5, diffusion on Ti_7S_{12} is along path 6, and diffusion on Ni_7S_{12} is along path 4 [Figure 5B]. This can be ascribed to the strong interlayer vdW interactions that impede the movement of Li ions along the interlayer. Therefore, Li ions prefer to diffuse along the surface instead of in the intercalation layer [Table 1].

To summarize, two ic-2Ds, i.e., Ti_7S_{12} and V_7S_{12} , are theoretically predicted to be promising ic-2D anode materials for LIBs because of their relatively higher lithium capacity (745.6 mA hg^{-1} for Ti_7S_{12} and 723.9 mA hg^{-1} for V_7S_{12}) and smaller Li diffusion barrier (0.17 eV surface barrier and 1.17 eV interlayer barrier for Ti_7S_{12} , 0.20 eV surface barrier and 0.92 eV interlayer barrier for V_7S_{12}). Besides, the metallicity of the two monolayers can be well maintained even after lithiation [Supplementary Figure 10], facilitating fast electron transfer.

Table 1. Comparison of Li diffusion barriers on the surface layer and interlayer and the theoretical capacities of ic-2Ds

	Ti ₇ S ₁₂	V ₇ S ₁₂	Cr ₇ S ₁₂	Mn ₇ S ₁₂	Fe ₇ S ₁₂	Co ₇ S ₁₂	Ni ₇ S ₁₂
Surface barrier (eV)	0.17	0.20	0.18	0.69	0.26	0.18	0.27
Interlayer barrier (eV)	1.17	0.92	0.58	1.58	0.64	0.74	0.97
Capacity (mA hg ⁻¹)	745.6	723.9	286.7	69.7	69.2	269.1	370.9

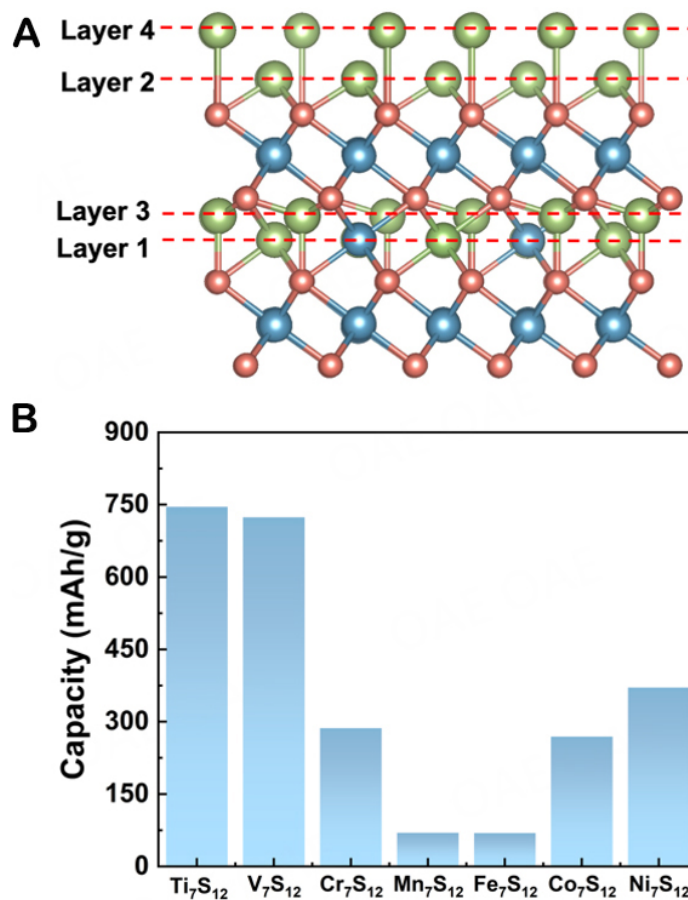


Figure 4. (A) A schematic geometric structure of ic-2D with lithium atoms adsorbed at two layers on one side and two intercalated and (B) maximum theoretical capacity of ic-2Ds.

Electrocatalytic performance of ic-2D crystals

The interlayer potential barriers of vdW gaps in 2D TMDs have been widely proven to cause poor interlayer charge transport^[43,44]. We believe that filling the vdW gap in TMDs with intercalants would be beneficial to address this bottleneck and thus enhance the HER performance of TMDs^[45]. To demonstrate the capability of ic-2Ds as electrocatalysts, we evaluated their catalytic performance toward HER at different θ levels.

Similar to the case of lithium adsorption, here, three adsorption sites (S1, S2, S3) are considered typical ic-2Ds [Figure 6A and B]. Since a $2 \times 2 \times 1$ supercell of ic-2Ds contains 12 nonmetal atoms on the top layer of atoms, the hydrogen coverage (θ) is calculated to be $1/12 = 8.3\%$. At this low θ value, hydrogen prefers to be adsorbed on the S1 site for most ic-2Ds [Figure 6C], except for Ni₇S₁₂ [Supplementary Figure 11]. After hydrogen adsorption, the metallicity of ic-2Ds can also be maintained [Supplementary Figure 12], which is beneficial to electrocatalysis^[46,47].

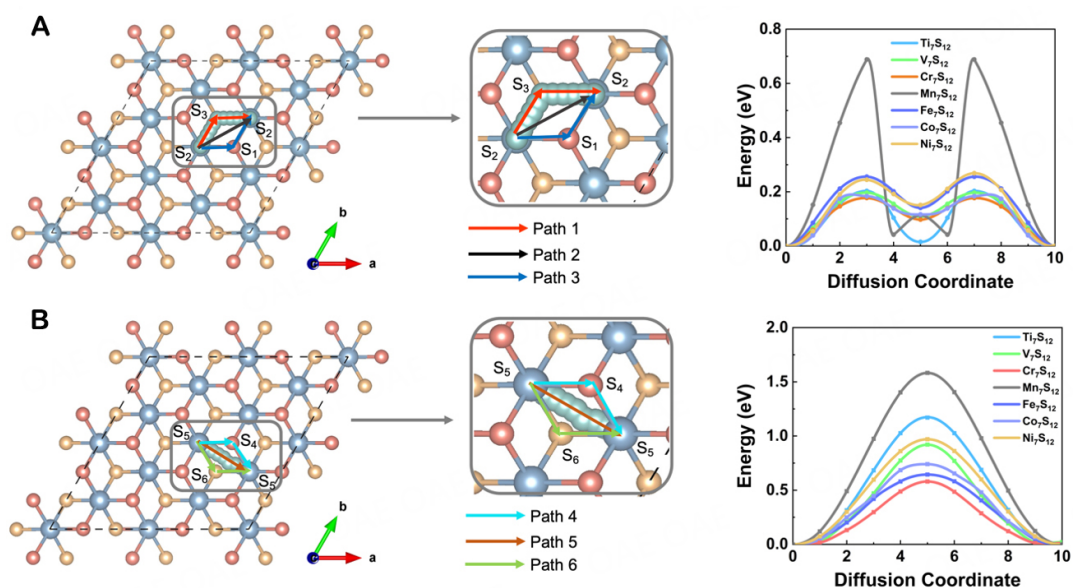


Figure 5. Schematic illustration of the possible diffusion paths of Li on ic-2Ds. (A) Top views of the three possible surface diffusion paths and the corresponding barriers for ic-2Ds. (B) Top views of the three possible interlayer diffusion paths and the corresponding barriers for ic-2Ds.

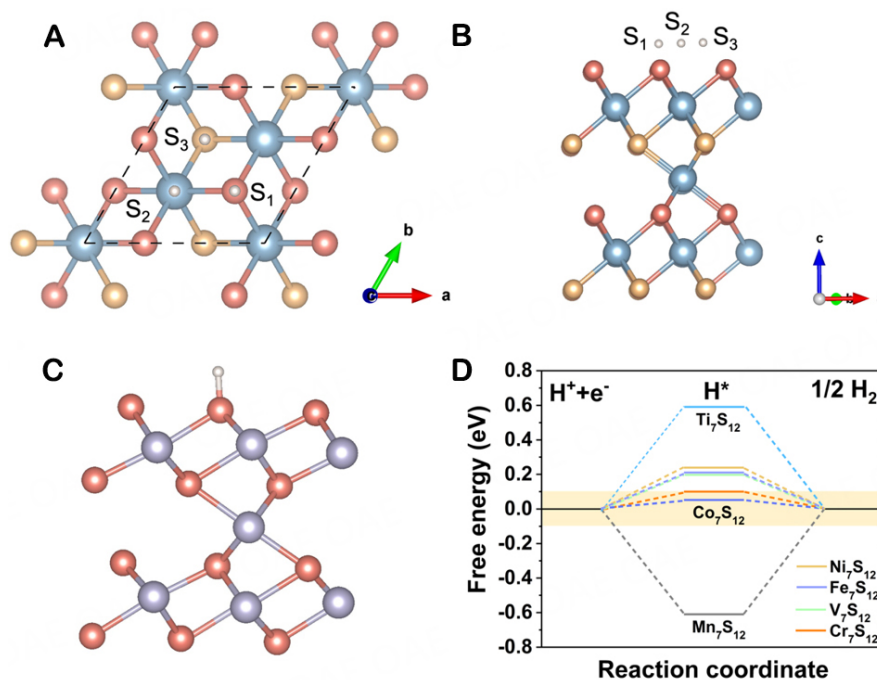


Figure 6. Possible active sites of H adsorption on ic-2Ds from the (A) top and (B) side views. (C) Optimized structure for H on Co₇S₁₂ at 8.3% coverage. (D) Hydrogen adsorption Gibbs free energy on ic-2Ds.

Computational screening for the potential HER electrocatalyst is based on the descriptor: the hydrogen adsorption Gibbs free energy (ΔG_{H}). According to the Sabatier principle^[48], an HER catalyst is promising when hydrogen is adsorbed on the catalyst surface neither too strongly nor too weakly, that is when ΔG_{H} is close to zero^[49-51]. In this work, the energetically most favorable configurations of hydrogen adsorbed on

ic-2Ds are adopted to calculate ΔG_{H} [Supplementary Table 5]. Among them, Ti_7S_{12} , V_7S_{12} , Fe_7S_{12} , and Ni_7S_{12} ic-2Ds bind H too weakly with large positive values of ΔG_{H} [Figure 6D], while Mn_7S_{12} binds H too strongly with the Gibbs free energy of -0.61 eV (which lead to difficult H desorption in the Heyrovsky/Tafel step). In comparison, Cr_7S_{12} (0.09 eV) and Co_7S_{12} (0.05 eV) bind H moderately with close-to-zero ΔG_{H} values, indicating that Cr_7S_{12} and Co_7S_{12} are excellent HER electrocatalysts under this θ and the adsorption free energy is mainly determined by the nonmetal element sulfur that binds hydrogen.

Since the θ also affects ΔG_{H} , here, we select Cr_7S_{12} and Co_7S_{12} to further study their catalytic performance at higher θ . According to our calculations, with θ increased from low (8.3%) to medium (25%) value, the ΔG_{H} values of Cr_7S_{12} and Co_7S_{12} increase up to 0.45 eV and 0.13 eV, respectively. When θ is further increased to full coverage (100.00%), both Cr_7S_{12} and Co_7S_{12} exhibit no bond with H because of the large positive value of ΔG_{H} [Supplementary Figure 13]. In general, Cr_7S_{12} and Co_7S_{12} can boost the HER at low θ but are not promising at high θ .

CONCLUSIONS

In summary, we explore the electrochemical properties of seven 3d ic-2Ds and their potential applications as the anode materials for LIBs and hydrogen reduction reaction processes by means of DFT computations. The band structure reveals the origin of the ferromagnetism behavior of Co_7S_{12} is from the intercalated Co atoms. For applications, Ti_7S_{12} and V_7S_{12} are identified as promising electrodes for LIBs due to their low Li diffusion barrier and high lithium capacity, while Cr_7S_{12} and Co_7S_{12} show good catalytic activity toward HER at low θ . The metallicity of these ic-2Ds ensures fast electron transport in the electrochemical processes. Overall, this study highlights the potential of ic-2D materials as a promising avenue for the development of sustainable energy storage systems.

DECLARATIONS

Authors' contributions

Conceptualization, methodology, writing-original draft: Fan K

Writing-review & editing, supervision, funding acquisition: Tsang YH, Huang H

Availability of data and materials

Supporting data for the findings presented in this work can be found in the [Supplementary Material](#). We hereby declare that: (1) This manuscript originates from the Ph.D. thesis of Dr. Ke Fan (first author). However, significant revisions have been made to the content, and substantial additional data have been incorporated into the current manuscript. (2) The reuse of certain data from the thesis in this journal publication adheres to the copyright regulations of the Hong Kong Polytechnic University.

Financial support and sponsorship

This work was supported by the Hong Kong Polytechnic University (ZE2F, CDBG, and 1-CD6V) and the Science and Technology Program of Guangdong Province of China (2021B1515130010).

Conflicts of interest

All authors declared that there are no conflicts of interest.

Ethical approval and consent to participate

Not applicable.

Consent for publication

Not applicable.

Copyright

© The Author(s) 2023.

REFERENCES

1. Chen H, Cong TN, Yang W, Tan C, Li Y, Ding Y. Progress in electrical energy storage system: a critical review. *Prog Nat Sci* 2009;19:291-312. [DOI](#)
2. Johansson TB, Burnham L. Renewable energy: sources for fuels and electricity. 1994. Available from: https://www.researchgate.net/publication/37402581_Renewable_Energy_Sources_for_Fuels_and_Electricity [Last accessed on 8 August 2023].
3. Yang Y, Bremner S, Menictas C, Kay M. Battery energy storage system size determination in renewable energy systems: a review. *Renew Sustain Energy Rev* 2018;91:109-25. [DOI](#)
4. Fan K, Ying Y, Lin Z, Tsang YH, Huang H. Building up an “elemental property - adsorption energy descriptor - decomposition barrier” three-tier model for screening biatom catalysts in sodium-sulfur batteries. *Adv Energy Mater* 2023;13:2370110. [DOI](#)
5. Larcher D, Tarascon JM. Towards greener and more sustainable batteries for electrical energy storage. *Nat Chem* 2015;7:19-29. [DOI](#) [PubMed](#)
6. Sun Y, Liu N, Cui Y. Promises and challenges of nanomaterials for lithium-based rechargeable batteries. *Nat Energy* 2016;1:16071. [DOI](#)
7. Martin G, Rentsch L, Höck M, Bertau M. Lithium market research - global supply, future demand and price development. *Energy Stor Mater* 2017;6:171-9. [DOI](#)
8. Fan K, Tsang YH, Huang H. Computational design of promising 2D electrode materials for Li-ion and Li-S battery applications. *Mater Rep Energy* 2023:100213. [DOI](#)
9. Zou X, Zhang Y. Noble metal-free hydrogen evolution catalysts for water splitting. *Chem Soc Rev* 2015;44:5148-80. [DOI](#) [PubMed](#)
10. Morales-Guio CG, Stern LA, Hu X. Nanostructured hydrotreating catalysts for electrochemical hydrogen evolution. *Chem Soc Rev* 2014;43:6555-69. [DOI](#) [PubMed](#)
11. Wang L, Wang L, Zhang L, Liu H, Yang J. Perspective of p-block single-atom catalysts for electrocatalysis. *Trends Chem* 2022;4:1135-48. [DOI](#)
12. Bai Y, Zhang H, Lu X, et al. Self-supported Ru-incorporated NiSe₂ for ampere-level current density hydrogen evolution. *Chemistry* 2023;29:e202300205. [DOI](#)
13. Zhu D, Zhang H, Miao J, et al. Strategies for designing more efficient electrocatalysts towards the urea oxidation reaction. *J Mater Chem A* 2022;10:3296-313. [DOI](#)
14. Xu K, Wang L, Xu X, Dou SX, Hao W, Du Y. Two dimensional bismuth-based layered materials for energy-related applications. *Energy Stor Mater* 2019;19:446-63. [DOI](#)
15. Manzeli S, Ovchinnikov D, Pasquier D, Yazyev OV, Kis A. 2D transition metal dichalcogenides. *Nat Rev Mater* 2017;2:17033. [DOI](#)
16. Chhowalla M, Shin HS, Eda G, Li LJ, Loh KP, Zhang H. The chemistry of two-dimensional layered transition metal dichalcogenide nanosheets. *Nat Chem* 2013;5:263-75. [DOI](#) [PubMed](#)
17. Fan K, Huang H. Two-dimensional host materials for lithium-sulfur batteries: a review and perspective. *Energy Stor Mater* 2022;50:696-717. [DOI](#)
18. Attanayake NH, Thenuwara AC, Patra A, et al. Effect of intercalated metals on the electrocatalytic activity of 1T-MoS₂ for the hydrogen evolution reaction. *ACS Energy Lett* 2017;3:7-13. [DOI](#)
19. Chen Z, Leng K, Zhao X, et al. Interface confined hydrogen evolution reaction in zero valent metal nanoparticles-intercalated molybdenum disulfide. *Nat Commun* 2017;8:14548. [DOI](#) [PubMed](#) [PMC](#)
20. Kwon IS, Kwak IH, Abbas HG, et al. Intercalation of aromatic amine for the 2H-1T' phase transition of MoS₂ by experiments and calculations. *Nanoscale* 2018;10:11349-56. [DOI](#)
21. Wu L, Dzade NY, Yu M, et al. Unraveling the role of lithium in enhancing the hydrogen evolution activity of MoS₂: intercalation versus adsorption. *ACS Energy Lett* 2019;4:1733-40. [DOI](#)
22. Zhao X, Song P, Wang C, et al. Engineering covalently bonded 2D layered materials by self-intercalation. *Nature* 2020;581:171-7. [DOI](#)
23. Fan K. Theoretical investigation of two-dimensional materials as promising electrode materials for Li-ion and Li-S batteries. 2022. Available from: <https://theses.lib.polyu.edu.hk/handle/200/11777> [Last accessed on 8 August 2023].
24. Kresse G, Furthmüller J. Efficient iterative schemes for ab initio total-energy calculations using a plane-wave basis set. *Phys Rev B* 1996;54:11169. [DOI](#)
25. Perdew JP, Burke K, Ernzerhof M. Generalized gradient approximation made simple. *Phys Rev Lett* 1996;77:3865. [DOI](#) [PubMed](#)
26. Grimme S. Semiempirical GGA-type density functional constructed with a long-range dispersion correction. *J Comput Chem* 2006;27:1787-99. [DOI](#) [PubMed](#)

27. Tang W, Sanville E, Henkelman G. A grid-based Bader analysis algorithm without lattice bias. *J Phys Condens Matter* 2009;21:084204. DOI
28. Henkelman G, Uberuaga BP, Jónsson H. A climbing image nudged elastic band method for finding saddle points and minimum energy paths. *J Chem Phys* 2000;113:9901-4. DOI
29. Nosé S. A unified formulation of the constant temperature molecular dynamics methods. *J Chem Phys* 1984;81:511-9. DOI
30. Fan K, Ying Y, Li X, Luo X, Huang H. Theoretical investigation of V_3C_2 MXene as prospective high-capacity anode material for metal-ion (Li, Na, K, and Ca) batteries. *J Phys Chem C* 2019;123:18207-14. DOI
31. Fan K, Ying Y, Luo X, Huang H. Monolayer PC_5/PC_6 : promising anode materials for lithium-ion batteries. *Phys Chem Chem Phys* 2020;22:16665-71. DOI
32. Nørskov JK, Bligaard T, Logadottir A, et al. Trends in the exchange current for hydrogen evolution. *J Electrochem Soc* 2005;152:J23. DOI
33. Ying Y, Fan K, Qiao J, Huang H. Rational design of atomic site catalysts for electrocatalytic nitrogen reduction reaction: one step closer to optimum activity and selectivity. *Electrochem Energy Rev* 2022;5:6. DOI
34. Mouhat F, Coudert FX. Necessary and sufficient elastic stability conditions in various crystal systems. *Phys Rev B* 2014;90:224104. DOI
35. Ying Y, Fan K, Luo X, Qiao J, Huang H. Transition metal-tetracyanoquinodimethane monolayers as single-atom catalysts for the electrocatalytic nitrogen reduction reaction. *Mater Adv* 2020;1:1285-92. DOI
36. Fan K, Ying Y, Luo X, Huang H. Nitride MXenes as sulfur hosts for thermodynamic and kinetic suppression of polysulfide shuttling: a computational study. *J Mater Chem A* 2021;9:25391-8. DOI
37. Ying Y, Lin Z, Huang H. "Edge/basal plane half-reaction separation" mechanism of two-dimensional materials for photocatalytic water splitting. *ACS Energy Lett* 2023;8:1416-23. DOI
38. Xie LM. Two-dimensional transition metal dichalcogenide alloys: preparation, characterization and applications. *Nanoscale* 2015;7:18392-401. DOI
39. Zhang X, Lai Z, Ma Q, Zhang H. Novel structured transition metal dichalcogenide nanosheets. *Chem Soc Rev* 2018;47:3301-38. DOI PubMed
40. Guan Z, Ni S, Hu S. Tunable electronic and optical properties of monolayer and multilayer janus MoSSe as a photocatalyst for solar water splitting: a first-principles study. *J Phys Chem C* 2018;122:6209-16. DOI
41. Enyashin AN, Yadgarov L, Houben L, et al. New route for stabilization of 1T- WS_2 and MoS_2 phases. *J Phys Chem C* 2011;115:24586-91. DOI
42. Tang Q, Jiang DE. Stabilization and band-gap tuning of the 1T- MoS_2 monolayer by covalent functionalization. *Chem Mater* 2015;27:3743-8. DOI
43. Chia X, Ambrosi A, Lazar P, Sofer Z, Pumera M. Electrocatalysis of layered group 5 metallic transition metal dichalcogenides (MX_2 , $M = V, Nb$, and Ta ; $X = S, Se$, and Te). *J Mater Chem A* 2016;4:14241-53. DOI
44. Lin L, Sherrell P, Liu Y, et al. Engineered 2D transition metal dichalcogenides - a vision of viable hydrogen evolution reaction catalysis. *Adv Energy Mater* 2020;10:1903870. DOI
45. Kwak IH, Kwon IS, Abbas HG, et al. Intercalated complexes of 1T'- MoS_2 nanosheets with alkylated phenylenediamines as excellent catalysts for electrochemical hydrogen evolution. *J Mater Chem A* 2019;7:2334-43. DOI
46. Ying Y, Fan K, Luo X, Huang H. Predicting two-dimensional pentagonal transition metal monophosphides for efficient electrocatalytic nitrogen reduction. *J Mater Chem A* 2019;7:11444-51. DOI
47. Ying Y, Fan K, Luo X, Qiao J, Huang H. Unravelling the origin of bifunctional OER/ORR activity for single-atom catalysts supported on C_2N by DFT and machine learning. *J Mater Chem A* 2021;9:16860-7. DOI
48. Rothenberg G. Catalysis: concepts and green applications. Hoboken, NJ: John Wiley & Sons; 2017.
49. Seh ZW, Kibsgaard J, Dickens CF, Chorkendorff I, Nørskov JK, Jaramillo TF. Combining theory and experiment in electrocatalysis: insights into materials design. *Science* 2017;355:eaad4998. DOI PubMed
50. Ying Y, Fan K, Zhu S, Luo X, Huang H. Theoretical investigation of monolayer $RhTeCl$ semiconductors as photocatalysts for water splitting. *J Phys Chem C* 2020;124:639-46. DOI
51. Ying Y, Luo X, Qiao J, Huang H. "More is different:" synergistic effect and structural engineering in double-atom catalysts. *Adv Funct Mater* 2021;31:2007423. DOI